Center for Turbulence Research
Proceedings of the Summer Program 2008

Boundary layer transition in high-speed flow

By P. A. Durbin†, J. W. Joo† AND O. Marxen

The framework is developed for studying discrete and continuous mode transition in high speed boundary layers. Linear modes are generated and separated into various types in order to specify acoustic, vortical, discrete or continuous components at the inlet. Implementation into a simulation code is discussed.

1. Introduction

Forces on, and heating of, high-speed vehicles depend critically on the location of transition to turbulence. Uncertainties in the physics, lack of experimental data, and the inability to model it, make transition a key outstanding problem in high-speed aerodynamics.

At the same time this is an extremely challenging regime to study through laboratory experiments. Noise sources are notoriously difficult to control because acoustic noise is in the same frequency range as shear-layer eigenmodes. Measurements within the flow are difficult at supersonic speeds. Real-gas effects are difficult to produce, except in short duration, shock tube facilities; etc. This experimental intransigence makes high-speed transition an excellent problem to study using computer simulation.

Significant uncertainty exists regarding the nature of transition between laminar and turbulent flow at supersonic speeds. Stetson (1992) provides a comprehensive review of experiments and theory. He notes many discrepancies between them, and indeed, that linear theory does not lead to prediction of transition, *per se*. The theory that he cites is linear analysis of *exponential instability*. There is a good deal of evidence that perturbations grow within the boundary layer, upstream of the neutral stability point; that is, disturbances grow in a region where all modal disturbances are exponentially *damped*. In experiments, this behavior is seen at low frequencies: Energy spectra in Graziosi & Brown (2002) show substantial growth in a broad band of frequencies, well below the linear instability modes. Although the Mack (e.g., Mack 1975) second-mode instability was seen, the dominant growth of energy was at significantly lower frequencies.

Boundary layer transition in incompressible flow has commonly been divided into "natural" and "bypass" types. That division has proved to be unapt: So-called natural transition is usually seen under well controlled conditions, often with artificial forcing. In the presence of environmental disturbances, bypass transition is far more common.

Further ambiguity is created by the notion that something is being "bypassed". Sometimes the term bypass is synonymous with *subcritical* instability; more often it alludes to transition beneath free stream disturbances. A more recent perspective on incompressible boundary layer transition has evolved from a recognition that Orr-Sommerfeld theory applies both to natural transition and to transition beneath free stream turbulence. Given that understanding, the two cases are characterized as *discrete* and *continuous* mode transition (Durbin & Wu 2007). Of course, Orr-Sommerfeld theory only describes linear processes. The connection to transition is far from obvious. They have been connected via

† Department of Aerospace Engineering, Iowa State University

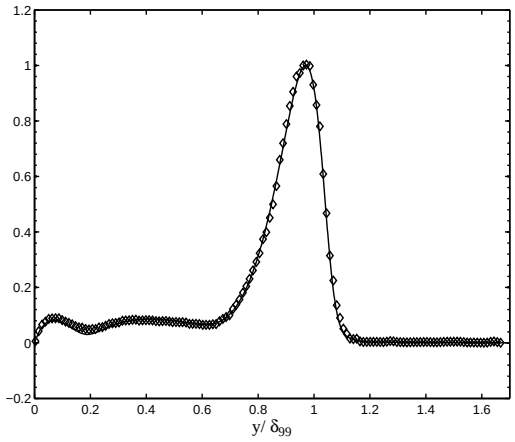

FIGURE 1. Comparison of $|\theta|$ at Ma=10, $\alpha = 0.12$, $\beta = 0$, $R = 1,000$ to $\diamond$ (Malik 1990). —— present.

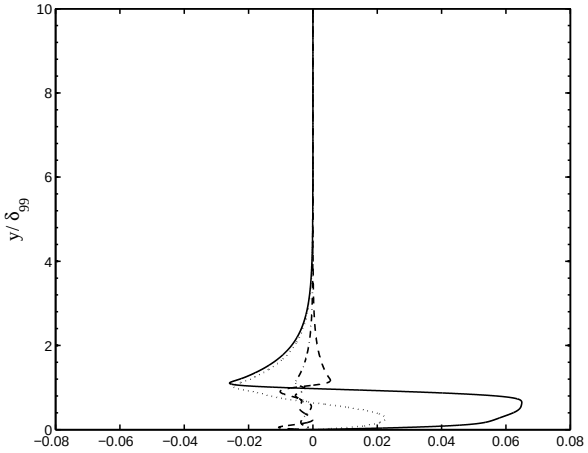

FIGURE 2. Second Mack mode: —— real part of u; - - - - imaginary part of u —·— real part of v; ····· imaginary part of v.

computer simulations. Subtleties have been found which were not anticipated by linear theory. A compliment of linear theory and computer simulation has proved effective in incompressible flow.

2. Eigenmodes and boundary conditions

Compressible eigenmodes are obtained as solutions to linearized, primitive equations (Malik 1990; Mack 1975). Assuming a disturbance proportional to

$$e^{ik_x x + ik_z z - i\omega t}$$

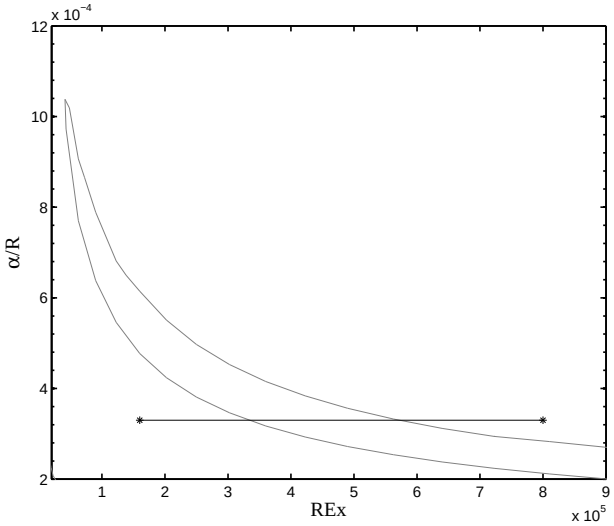

FIGURE 3. Neutral stability curve for Ma=4.5,Pr=0.72, 2nd Mack mode region. The dashed line indicates the extent of the present DNS domain for the discrete mode. ($\alpha = 0.132$, $\omega = 0.1172$)

provides the linear stability equations. If the dependent variables multiplying this complex exponential form the vector

$$\phi(y) = \begin{pmatrix} u \\ v \\ p \\ \theta \\ w \end{pmatrix} \tag{2.1}$$

of velocity, pressure and temperature, then the governing equations have the form

$$\boldsymbol{A} \cdot \frac{d^2\phi}{dy^2} + \boldsymbol{B} \cdot \frac{d\phi}{dy} + \boldsymbol{C}\phi = 0. \tag{2.2}$$

This is an eighth order equation because of the form of $\boldsymbol{A}$, or because it can be re-written with the dependent variable

$$\psi = \begin{pmatrix} u \\ d_y u \\ v \\ p \\ \theta \\ d_y\theta \\ w \\ d_y w \end{pmatrix} \tag{2.3}$$

in the form

$$\boldsymbol{D} \cdot \frac{d\psi}{dy} + \boldsymbol{E}\psi = 0. \tag{2.4}$$

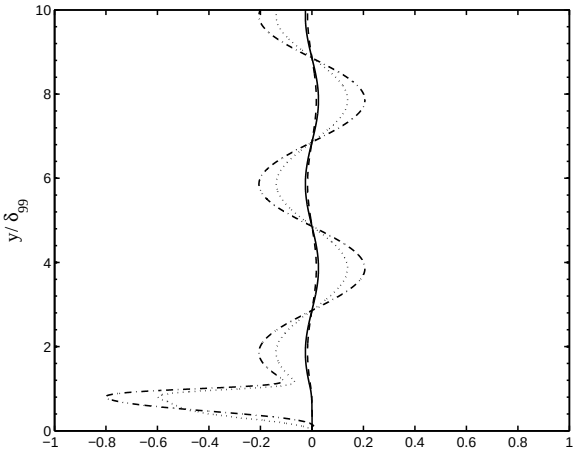

FIGURE 4. Subsonic acoustic mode: ——— real part of p; – – – – imaginary part of p —·— real part of θ; ····· imaginary part of θ.

The coefficients are functions of ω, k_x and y, as presented in Malik (1990). They also depend on Mach, M, and Reynolds number, R. These are based on free stream: $M = U_\infty/c_\infty$, $R = \sqrt{U_\infty x/\nu_\infty}$.

The eigenvalues, k_x for spatial evolution, or ω for temporal evolution, are complex. They separate into two families, discrete and continuous.

For the discrete mode, the eight boundary conditions are

$$(u, v, w, \theta)_1 = 0 = (u, v, w, \theta)_N$$

at the wall and uppermost grid point. Eqs. (2.2) are discretized by fourth order central differences. This provides an eigenvalue problem , e.g. for fixed k_x, that is solved with the Lapack CGGEV routine. Once an unstable eigenvalue is found, a more accurate solution is obtained with a finer grid and a Newton's method search. At present, discrete modes are temporal (real $k_x = \alpha$), with spatial growth approximated by Gaster's transformation. Fig. 1 verifies the present solver by comparison to Malik (1990). Fig. 2 shows the solution for the second Mack mode eigenfunction. Fig. 3 shows the stability region, with a dashed line showing the extent of the DNS domain, aligned with the α for this mode. It crosses the upper and lower branches.

The continuous modes require more attention to the free stream condition; the wall condition is unchanged. In the uniform, free stream flow, a linear disturbance can be expressed as a sum of eigenmodes. These can be thought of as vorticity, acoustic and entropy modes (Balakumar & Malik 1992), although that is not invoked here. Following Mack (1975) and Balakumar & Malik (1992), let the solution vector be (2.3). In the free stream the linearized compressible flow eqs. (2.4) have constant coefficients. If a vertical wavenumber, k_y is prescribed, they have the eight eigenvalues λ_i. For instance

$$\lambda_1 = \lambda_2 = i(k_x - \omega)Re + k_x^2 + k_z^2 \tag{2.5}$$

The remaining λ's can be found in Balakumar & Malik (1992). If λ_1 is set to $-k_y^2$ and

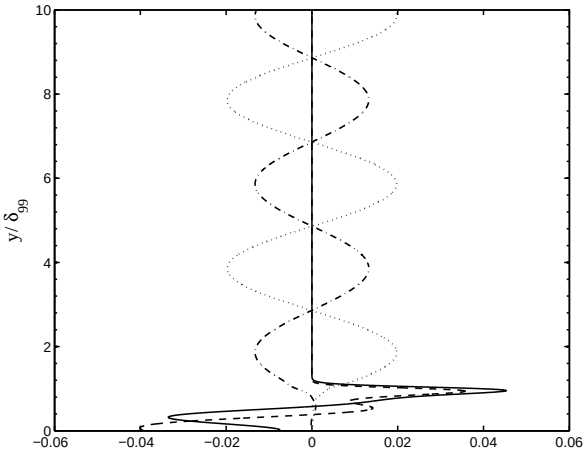

FIGURE 5. Subsonic acoustic mode: ——— real part of z-vorticity; – – – – imaginary part of z-vorticity; —·— real part of dilation; ····· imaginary part of dilation.

the corresponding formula is inverted to find k_x,

$$k_x^r = \omega \left[\sqrt{M^2 + \frac{4\omega^2}{Re^2}} + M \right]^{-1/2}; \qquad k_x^i = \frac{Re}{2} \left[\frac{\omega}{k_x^r} - 1 \right] \tag{2.6}$$

is found, where

$$M = \frac{1}{2} + \frac{2(k_y^2 + k_z^2)}{Re^2}.$$

This k_x, substituted into the formulas for the λ's, gives $\lambda_i = -k_y^2$ for all except λ_4 and λ_3. Those equaling $-k_y^2$ are convective modes.

Two acoustic modes are also obtained with phase speeds $U_\infty \pm c_\infty$. They propagate at an angle to the flow. λ_4 and λ_3 are the acoustic modes. For the k_x of convective modes, they are not equal to $-k_y^2$; however, they are the squared vertical wavenumber of the corresponding acoustic modes. Alternatively, particular acoustic modes are obtained by setting either λ_4 or λ_3 to $-k_y^2$ and solving for the corresponding k_x.

The eigenvectors, $\xi^{(i)}$, corresponding to the eigenvalues λ_i are used to obtain four boundary conditions for continuous modes. The eigenvectors are known in closed form (Mack 1975). For instance

$$\boldsymbol{\xi}^{(3)} = \begin{pmatrix} -ik_x \\ -ik_x\sqrt{\lambda_1} \\ \sqrt{1 - M^2(1-c)^2} \\ ik_x(1-c) \\ ik_x(\gamma-1)M^2(1-c) \\ ik_x(\gamma-1)M^2(1-c)\sqrt{\lambda_3} \\ 0 \\ 0 \end{pmatrix}$$

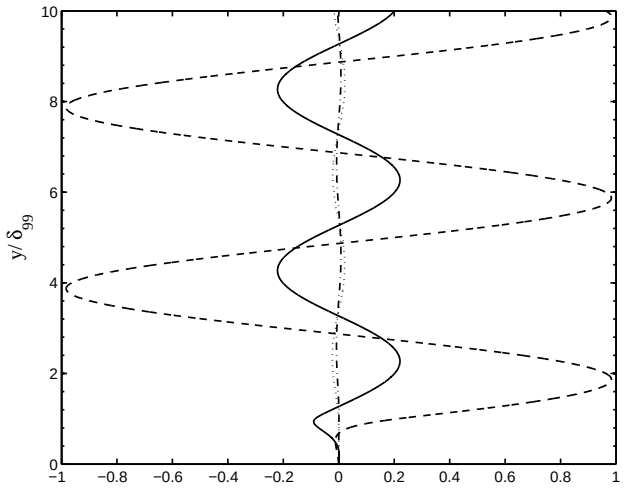

FIGURE 6. Vorticity mode: ——— real part of u; – – – – imaginary part of u; —·— real part of v; ····· imaginary part of v.

where $c = \omega/k_x$ is the complex wave speed and M is the Mach number. At large y the solution behaves as

$$\boldsymbol{\Psi} = \sum_{1}^{8} A_i \boldsymbol{\xi}^{(i)} e^{\sqrt{\lambda_i} y}. \tag{2.7}$$

Let the matrix of eigenvectors be

$$\boldsymbol{E} = \left\{ \boldsymbol{\xi}^{(1)}, \boldsymbol{\xi}^{(2)} \ldots \boldsymbol{\xi}^{(8)} \right\}$$

or, in component form

$$E_{ij} = \xi_j^{(i)}.$$

The far-field conditions are formulated in terms of its inverse E_{ij}^{-1}. Note that $E_{ik}^{-1} \xi_k^{(j)} = \delta_{ij}$. Hence, the coefficients in eq. (2.7) are

$$A_i = E_{ik}^{-1} \Psi_k e^{-\sqrt{\lambda_i} y}.$$

One of the acoustic modes has exponential growth with y and its amplitude must be set to zero. This is mode 4. The other acoustic mode is mode 3. We identify modes 5 and 6 with entropy. Thus a vorticity mode can be defined by setting the amplitudes of modes 4,5,6 to zero and normalizing another amplitude to unity:

$$\begin{aligned} E_{4k}^{-1} \Psi_k &= 0 \\ E_{5k}^{-1} \Psi_k &= 0 \\ E_{6k}^{-1} \Psi_k &= 0 \\ E_{1k}^{-1} \Psi_k e^{-\sqrt{\lambda_1} y} &= 1. \end{aligned} \tag{2.8}$$

These four far-field conditions are equivalent to four relations between the the dependent

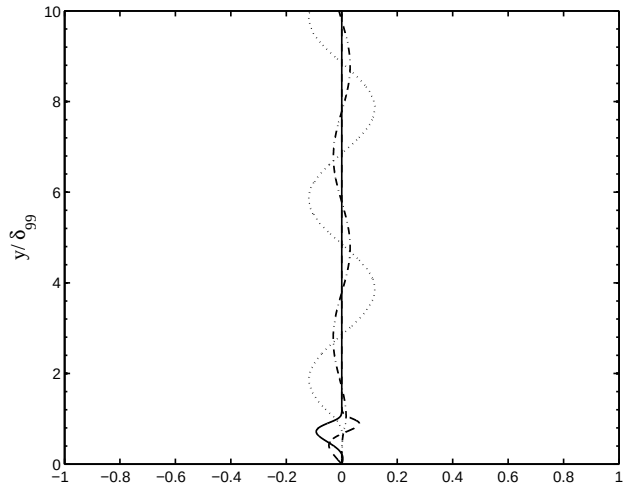

FIGURE 7. Vorticity mode, ——— real part of θ, dashed : imaginary part of θ —·— real part of w, ····· imaginary part of w.

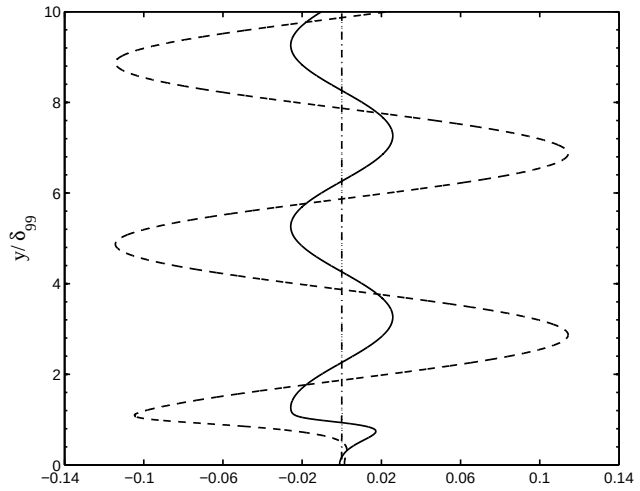

FIGURE 8. Vorticity mode, ——— real part of z-vorticity, dashed : imaginary part of z-vorticity —·— , real part of dilation, ····· imaginary part of dilation.

variables and their derivatives (see eq. 2.3). The latter are approximated by one-sided differences at the two uppermost grid points.

The formulation in eq. (2.8) has some similarity to the method of Balakumar & Malik (1992). However, they assumed that four of the eight λ_i's had positive real parts, so eq. (2.8) is replaced by the four even numbered amplitudes being zero.

In continuous mode transition, modes are stable. Their eigenvalues are not the key to

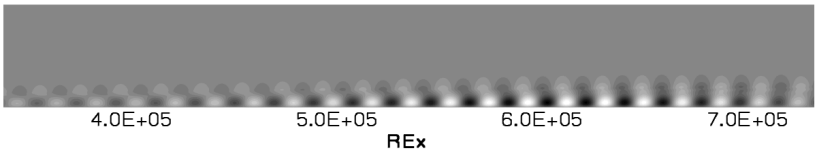

FIGURE 9. u' disturbance contour, for the discrete mode showing growth of the disturbance.

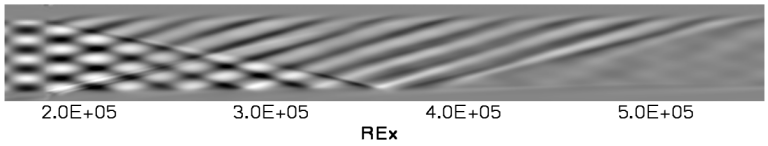

FIGURE 10. Dilation contours at z-normal plane, contour level is arbitrary, before improved treatment of the upper sponge region.

how they effect transition; rather it is their y-profiles that play a critical role in determining interaction between the boundary layer and external perturbations. By contrast, in discrete mode transition, the complex dispersion relation is of primary importance, especially the unstable modes.

Various modes are computed by choice of the set of null amplitudes in equation 2.8. Figs. 4 to 8 display solutions for acoustic and vorticity modes.

3. Non-linear computations

The linear eigen solutions provide a basis for the inflow disturbance. The flow code (Nagaragan 2004) uses a large stencil to achieve high-order accuracy. The linear solution was imposed on the first six grid points to fill the stencil. The spatial evolution was provided by the linear solution. Without doing this, the perturbation did not enter the flow domain smoothly. Our ultimate objective is to simulate boundary layer response to inlet disturbances, leading to transition to turbulence. As of yet, only preliminary computations have been done.

Development of the discrete mode is shown in fig. 9. This provides a verification of the simulation code. The growth follows the linear theory prediction. Note that at the far right the disturbance enters into a numerical "sponge" region.

A difficulty was encountered with the acoustic mode. The sponge at the top of the domain prevented incoming waves. These are required to correctly simulate acoustic modes. The fix was to prescribe the linear solution in the sponge region. The problem and correction are displayed in figs. 10 and 11. Perturbation of the boundary layer by acoustic modes is illustrated by figs. 12 to 15.

The vortical mode has proved difficult to generate without large contamination from the entropy mode. Fig. 16 is a simulation with this mode, as it presently stands. In this vorticity mode, entropy components are eliminated (fig. 6 and equation 2.8). But, as a result, the Squire mode becomes very large and Orr-Sommerfeld becomes small; this has the effect of producing only a small perturbation inside the boundary layer.

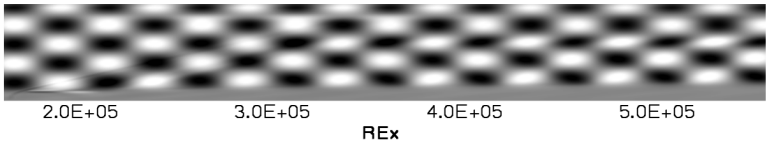

FIGURE 11. Dilation contours at z-normal plane, contour level is arbitrary, with improved treatment of the upper sponge region.

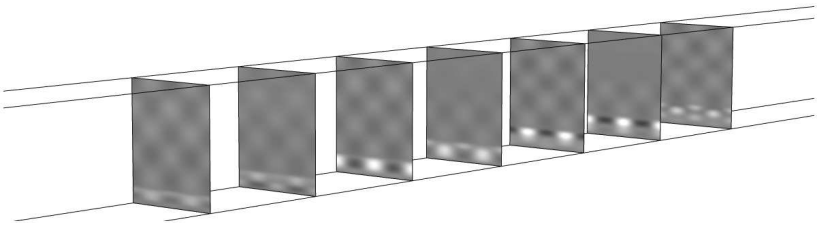

FIGURE 12. Continuous acoustic mode u disturbance contours for $-0.01 < u' < 0.01$ in planes normal to x.

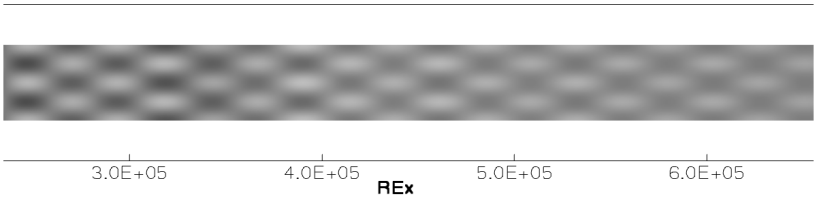

FIGURE 13. Acoustic mode u disturbance contours for $-0.01 < u' < 0.01$ in plane $y = 0.3\delta$.

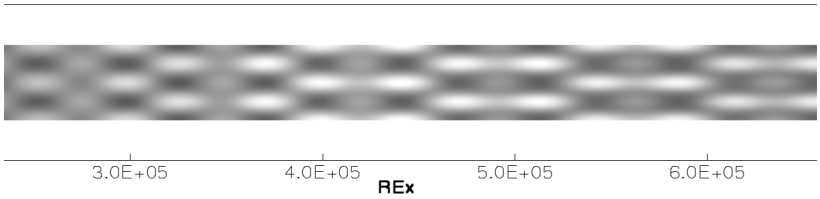

FIGURE 14. Acoustic mode u disturbance contours for $-0.01 < u' < 0.01$ in plane $y = \delta$.

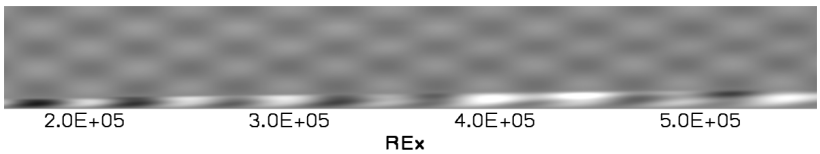

FIGURE 15. Acoustic mode u disturbance contours for $-0.01 < u' < 0.01$ in xy-plane.

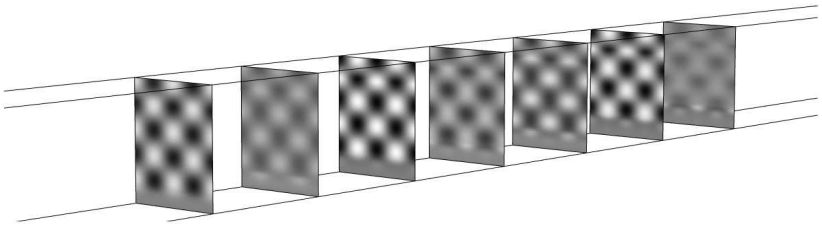

FIGURE 16. Vorticity mode. u-contours for $-0.034 < u' < 0.034$.

REFERENCES

BALAKUMAR, P. & MALIK, M. R. 1992 Discrete modes and continuous spectra in supersonic boundary layers, *J. Fluid Mech.* **239**, 631–656.

DURBIN, P.A. & WU, X. 2007 Transition beneath vortical disturbances, *Ann. Rev. Fluid Mech.* **39**, 107–128.

FEDOROV, A. V. & TUMIN, A. 2003 Initial-value problem for hypersonic boundary layer flows, *AIAA J.* **41**, 379–389.

GRAZIOSI, P. & BROWN, G.L. 2002 Experiments on stability and transition at Mach 3, *J. Fluid Mech.* **472** 83–124.

LIU, Y., ZAKI, T.A. & DURBIN, P.A. 2008 Boundary Layer Transition by Interaction of Discrete and Continuous Modes, *J. Fluid Mech.* **604** 199–233.

MACK, L. M. 1975 Linear stability theory and the problem of supersonic boundary-layer transition, *AIAA J.* **3**, 278–289

MALIK, M. R. 1990 Finite difference solution of the compressible stability eigenvalue problem, *NASA* **16572**.

NAGARAJAN, S. 2004 Leading edge effects in bypass transition. PhD thesis, Mechanical Engineering, Stanford University.

STETSON, K.F. 1992 Hypersonic boundary layer transition, *Advances in Hypersonics v.1*, J.J. Bertin, R. Glowinski, J. Periaux, eds. Birkhauser publications, 324–417.